European Polymer Journal 173 (2022) 111256

Contents lists available at ScienceDirect

European Polymer Journal

journal homepage: www.elsevier.com/locate/europolj

3D printable hybrid acrylate-epoxy dynamic networks

J. Casado [a], O. Konuray [a,*], A. Roig [b], X. Fernández-Francos [a], X. Ramis [a]

[a] Thermodynamics Lab, ETSEIB – UPC, Avda. Diagonal 647, 08028 Barcelona, Spain
[b] Dept. of Analytical and Organic Chemistry, Universitat Rovira I Virgili, C/ Marcel·lí Domingo, 1. 43007 Tarragona, Spain

ARTICLE INFO

Keywords:
Covalent adaptable network
Vitrimer
3D printing
Beta-hydroxy ester
Dual-cure

ABSTRACT

Polymer networks with dynamic bonds, also known as covalent adaptable networks (CANs) combine the superior mechanical properties and chemical resistance of thermosets with the ability to be reprocessed, a feat formerly attributed only to thermoplastics. Inspired by an evergrowing body of research on dynamic poly(β-hydroxy ester) networks, a polyacrylate/epoxy-acid thermoset was designed, which contains a high concentration of β-hydroxy ester bonds that partake in transesterification reactions that facilitate the repair and recycle of the cured material at feasible temperatures. Firstly, liquid formulations are subjected to UV light to initiate acrylate homopolymerization to obtain the intermediate, partially-cured material. A subsequent thermal treatment triggers the epoxy-acid reaction, which improves the mechanical properties and helps increase the likelihood of transesterifications as new β-hydroxy ester groups are formed. The effect of thermal post-treatment and the choice of catalyst on viscoelastic properties and stress relaxation behavior of these materials is studied. Results show that, transesterification reactions reach equilibrium in less than 4 h at 180 °C during which time the overall crosslinking density increases further. As to the choice of catalyst, a commonly used zinc acetylacetonate outperforms an imidazole-type base. Thanks to the dynamic bonds, damaged samples can be repaired fully using simple procedures. Recyclability is tested by grinding pristine samples and re-molding them under pressure and temperature. Practically complete recovery of viscoelastic properties is confirmed.

1. Introduction

Covalent adaptable networks (CANs) are thermosetting polymers featuring covalent bonds that are able to reshuffle through exchange reactions triggered using appropriate stimuli, such as heat. Given that the overall network connectivity is maintained during these exchange reactions, the thermoset acquires a certain malleability and reparability when heated, which are abilities formerly attributed exclusively to thermoplastics. The definition of CANs was introduced more than a decade ago by Kloxin et al. [1] and possible exchange mechanisms that underlie CANs have been reviewed in detail [2]. Furthermore, there are excellent reviews that treat the subject of CANs at the material level, with consideration of mechanical properties [3,4] and also with respect to possible applications such as biomaterials and additive manufacturing [5,6]. As a matter of fact, CANs that can maintain their network connectivity while undergoing exchange reactions, and thus exhibit an Arrhenius-like flow behavior when heated, were given the name "vitrimers", since this behavior is akin to vitreous silica. The first reported vitrimer was a poly(hydroxy ester) based network which underwent transesterification when heated [7].

In the realm of ester based dynamic networks, zinc salts are commonly employed as transesterification catalysts. An epoxy-acid reprocessable material with zinc acetoacetate as catalyst was described by Yu et al wherein they study the effect of reprocessing conditions (such as temperature, time, and pressure), and multiple reprocessing on mechanical properties [8]. In another work, Niu et al copolymerized vinyl monomers to obtain carboxyl and zinc carboxylate containing pre-polymers that were later post-cured using DGEBA [9]. The Zn^{2+} ions catalyze transesterification, enabling reprocessability. The catalysis of transesterification by zinc salts was also documented in epoxy vitrimers [7,10,11] or other β-hydroxy ester containing polymers [12]. The presence of hydroxyl groups in the matrix is reported to enhance transesterification rate. In fact, neighboring β-hydroxyls enhance reprocessability up to 10 times [13], apparently through a mechanism in which the hydrogen bond forming in the β-hydroxyl containing structures renders the carbonyl carbon more electrophilic, thereby facilitating attack by the electrophile such as alcohol (R-OH) [14]. In the extreme case (i.e. when they are abundant) they might

* Corresponding author.
E-mail address: ali.osman.konuray@upc.edu (O. Konuray).

https://doi.org/10.1016/j.eurpolymj.2022.111256
Received 11 March 2022; Received in revised form 28 April 2022; Accepted 5 May 2022
Available online 10 May 2022

alleviate altogether the need for a catalyst. One such example of a catalyst-free epoxy vitrimer was demonstrated by Han et al [15].

CANs synthesized from photocurable monomers have been evaluated in stereolithography based 3D printing applications which conventionally rely on non-recylable thermosets. The introduction of CANs thus can help alleviate the carbon footprint of these 3D printed products. While most stereolithographically 3D printed CANs reported so far are based on acrylate photopolymerization [12,16], some are based on thiol-acrylate click chemistry [17,18]. Two-component CANs printed by purely thermal, extrusion-based methods are also reported, along with many dual-cure and 3D printable CANs [19]. In this latter group of materials, an acrylate based component is firstly cured in a stereolithography-based process, such as in a digital light processing (DLP) printer. After that the printed object is thermally treated to cure a secondary monomer in the system which can be, among other possibilities, an epoxide [20] or a polyurethane [21].

Inspired by all the above, in this work, we have formulated a hybrid acrylate-epoxy CAN that can be printed in a DLP printer. The process starts with a diacrylate monomer, namely glycerol 1,3-diglycerolate diacrylate (GLYDA), which undergoes radical-mediated acrylate homopolymerization to yield a tightly crosslinked polyacrylate network. The GLYDA molecule features two β-hydroxy ester groups and additional pendant hydroxyl groups along its aliphatic backbone. To the best of our knowledge, the use of a β-hydroxy ester containing acrylate in a hybrid CAN was not reported before. When the fully cured material is thermally treated, various transesterification reactions are expected to occur. These ester-ester or ester-hydroxyl exchanges can take place across all the β-hydroxy ester moieties present in the overall polymeric network. These moieties either originate from GLYDA itself, or form as a result of epoxy-acid reaction. The DLP cured objects are subsequently subjected to elevated temperatures to cure the epoxy component. Similar to other dual-cure systems previously described by our group, the properties at each curing stage can be tailored by changing monomer composition, according to processing and application requirements [22,23]. Following a well-established strategy to prepare vitrimers, two catalysts capable of promoting both the epoxy-acid reaction and the transesterification were used: a zinc acetylacetonate, $Zn(AcAc)_2$ [24], and 1-methylimidazole [25]. After a full characterization of curing kinetics and viscoelastic properties of the cured materials, we investigate the effect of catalyst and of thermal post-cure on the final viscolelastic properties and stress-relaxation behavior.

2. Materials and methods

The molecular structures of the chemicals used are given in Scheme 1. The formulations studied are given in Table 1.

All chemicals, except the epoxy resin (ER), were purchased from Sigma-Aldrich (Madrid, Spain) and used without purification. ER was kindly supplied by Po.Int.Er S.R.L. (Valfenera, Italy). Mixtures containing $Zn(AcAc)_2$ were prepared by dissolving the transesterification catalyst and photoinitiator (either TPO or DMPA) in the acrylate monomers at 60 °C, and then by adding ER and GLU at the same temperature. Mixtures were magnetically agitated until homogenization. When 1-MI was used, it was added at the end of the preparation after cooling down the mixture. Slightly turbid solutions were obtained in formulations with $Zn(AcAc)_2$ due possibly to its inherent incompatibility with the diacrylate. GMA was used as coupling agent between the polyacrylate and epoxy-acid networks to improve homogeneity. GMA/GLYDA acrylate molar ratio was 1:1. The molar ratio between acid groups (GLU) and epoxide groups (GMA + ER) was also 1:1. A different mixture, named Base-3D, was prepared by modifying the basic formulation with PEGMA (MW = 300 g mol^{-1}), such that the PEGMA:GLYDA weight ratio was 1:1. This was done to reduce viscosity so that the resin can be easily 3D printed. The addition of PEGMA was observed to promote the dispersion of $Zn(AcAc)_2$ during the preparation of the formulations and had a positive effect on network homogeneity as well (vide infra). The first curing stage was carried out using either of the following two methods: 1) using a Vilber-Lourmat UV oven and hand-made transparent molds with PTFE spacers, or 2) using a Asiga MAX UV385 DLP-3D printer (Base-3D). The second curing stage was carried out at 120 °C for 12 h in a Memmert convection oven to ensure complete cure. Thermal post-treatments at 180 °C were carried out also in the same oven.

A Mettler DSC3 + calorimeter was used to measure both the T_g and the polymerization heats. Photocuring experiments were performed using a Hamamatsu LC5 light source equipped with a Hg-Xe mid-pressure lamp adapted to a Mettler DSC821 calorimeter. UV light intensity was 36 mW cm^{-2} measured at 365 nm using a radiometer. Conversion of

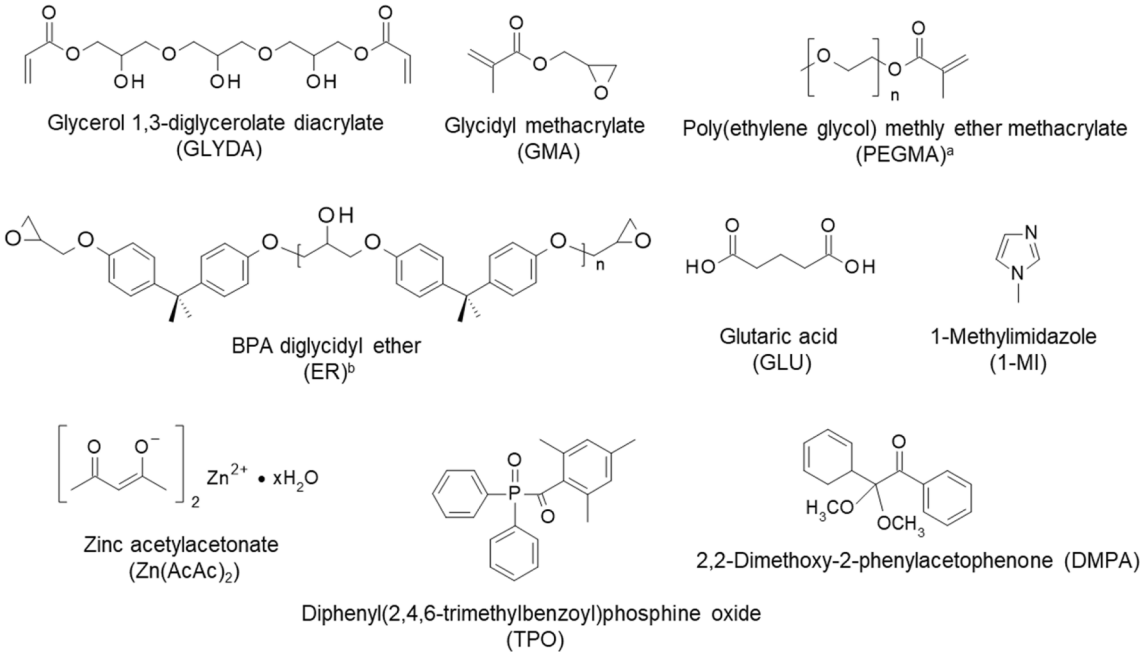

Scheme 1. Monomers catalysts and initiators used in the formulations. [a] MW = 300 g mol^{-1}, [b] Epoxy equivalent wt. = 187 g ee^{-1}.

Table 1
Composition of formulations based on 1 g of GLYDA. Catalyst loadings are given as wt. percentages.

Formulation	GLYDA (g)	PEGMA (g)	GMA (g)	ER (g)	GLU (g)	PI* (2%) (g)	$Zn(AcAc)_2$ (6%) (g)	1-MI (1%) (g)
Base-Zn	1.00	–	0.82	2.00	1.09	0.10	0.29	–
Base-MI	1.00	–	0.82	2.00	1.09	0.10	–	0.05
Base-Mix	1.00	–	0.82	2.00	1.09	0.10	0.29	0.05
Base-3D	1.00	1.00	0.82	2.00	1.09	0.12	0.35	–

*PI: Photoinitiator; either TPO or DMPA.

functional groups, defined as a function of time $x(t)$, was calculated using $x(t) = \Delta h(t)/\Delta h_{total}$ where $\Delta h(t)$ is the heat evolved up to time t, and Δh_{total} is the total polymerization heat. To probe the storage stability of intermediate (i.e. only photocured) samples, a different equation, namely $x = 1 - \Delta h_{residual}/\Delta h_{total}$ was used where Δh is the heat evolved during the cure of a sample stored for a known duration of time, and Δh_{total} is the total reaction heat of a freshly prepared and photocured sample.

The intermediate and final (i.e. fully cured material) T_g were taken as the half-way point of the heat capacity step observed in a scan at 10 °C min^{-1}, following the DIN 51,007 standard method.

Functional group conversions were also monitored using a temperature-controlled Brucker Vertex 70 FTIR spectrometer equipped with an attenuated total reflection (ATR) accessory (GoldenGate™, Specac Ltd.). The relevant wavelengths are marked on the spectra presented (vide infra). Spectra were collected in absorbance mode with a resolution of 4 cm^{-1} within the 600–4000 cm^{-1} wavelength range, averaging 20 scans for each spectrum. In photocuring tests, the same UV irradiation equipment with the same specifications as in DSC measurements was used.

A TA Instruments DMA Q800 device was used for thermomechanical analysis of cured samples. Prismatic samples with dimensions 1.5 × 10 × 30 mm^3 (thickness × width × length) were analyzed using a single cantilever clamp with a free length of 10 mm at a frequency of 1 Hz and amplitude of 15 μm at 3 °C min^{-1} from −50 °C up to the rubbery state to measure storage modulus, loss modulus, and tan delta. Stress relaxation experiments were performed on samples with dimensions 1.5x10x20 mm^3 using a 3-point bending configuration with a preload force of 0.01 N and a fixed strain of 1%. Flexural modulus was determined at 25 °C using a 3-point bending configuration with the same dimensions as in stress relaxation experiments, using the same preload force and a force ramp of 3 N/min.

Thermogravimetric analysis (TGA) was performed at 10 °C/min using a Mettler TGA/SDTA 851e/LF/1100 thermobalance. Fully cured samples were analyzed under isothermal conditions and under 50 cm^3 min^{-1} of nitrogen purge.

Reprocessing capability of the fully cured material was tested by finely chopping a sample and hot-pressing in a Specac Atlas manual 15 T hydraulic press at 9.25 MPa in an aluminum mold at about 180 °C for 5 h.

3. Results and discussion

3.1. Characterization of curing kinetics

FTIR spectra collected during the photocuring of Base-3D is given in Fig. 1. The disappearance of the acrylate and methacrylate bands at various wavelengths (marked on the figure) and the intactness of the epoxy band at 915 cm^{-1} confirms complete acrylate conversion (stage 1 curing) and no epoxy-acid reaction. Moreover, the carbonyl band at 1720 cm^{-1} (acrylate C=O) shifts to 1730 cm^{-1} (ester C=O), making the acid carbonyl characteristic peak at 1720 cm^{-1} visible, similar to what was observed in earlier works [26]. These observations suggest the only reaction taking place is the radical-mediated acrylate/methacrylate polymerization.

In Fig. 2, the FTIR spectra collected during thermal postcuring of a

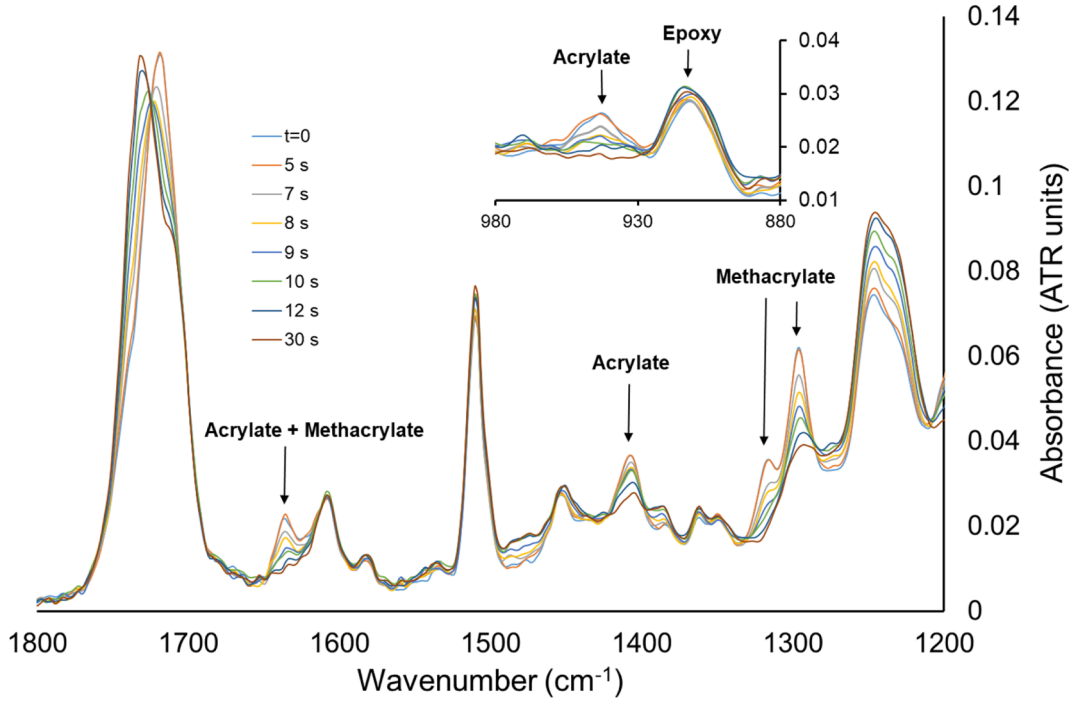

Fig. 1. FTIR spectra of the photocuring of Base-3D with UV light at 30 °C. Full acrylate + methacrylate conversion is achieved in 30 s.

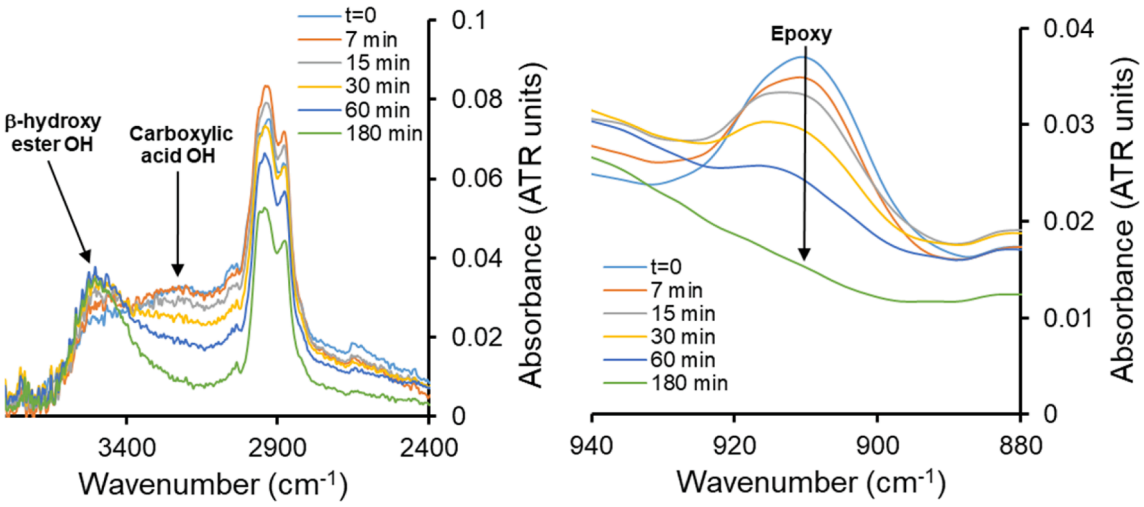

Fig. 2. Thermal (stage 2) curing of Base-3D at 120 °C monitored in FTIR. Hydoxyl formation due to new β-hydroxy ester bonds, and acid hydroxyl consumption is observed above 3000 cm^{-1} band (left) along with the disappearance of epoxy groups (right). 96% conversion is achieved in 180 min.

UV-cured Base-3D formulation at 120 °C can be seen. Practically complete conversion is achieved in 3 h. The disappearance of the carboxylic acid OH band and the appearance of the β-hydroxy ester OH band, together with the disappearance of the epoxy group, indicate that the second curing proceeds via the expected epoxy-acid reaction.

The first curing stage is complete in mere seconds (Fig. 1), while the second curing stage occurs at higher temperatures and at a rate several orders of magnitude lower. Globally, the curing takes place in two well-defined, sequential and orthogonal stages, similar to other 3D-printable dual-curing systems [27,28].

Comparing the curing rates of the two stages, one can confirm that thermal curing is the rate determining step in the processing of these materials. Although a fast curing reaction might prove practical, it might also jeopardize storage stability. The epoxy-acid reaction is not latent and thus a slow second curing stage might actually be crucial in terms of storage stability of the uncured mixtures and also intermediate stage materials. It is therefore interesting to study the effect of catalyst choice and formulation composition on this second curing stage.

In Fig. 3, DSC thermograms at various isotherms for the second curing stage of Base-3D are given. FTIR and DSC conversions are compared at 120 °C and a good fit is observed as can be seen. This suggests that the degree of cure can be determined accurately with either technique. In spite of the relatively slow curing kinetics, the second curing completes in approx. 1 hr at 140 °C.

To elucidate the kinetics of the epoxy-acid reaction, DSC data were analyzed using i) an integral isoconversional method and, ii) model-fitting. For the latter, an autocatalytic, Kamal-type model with a total reaction order of 2 was used (i.e. $n + m = 2$), similar to other epoxy-acid/anhydride reactions modeled earlier [29]. The reader is directed to the same reference for detailed explanations of both kinetic analysis methods. The isothermal isoconversional method is based on the assumption that reaction rate at a given conversion is solely a function of temperature, leading to the following linear expression.

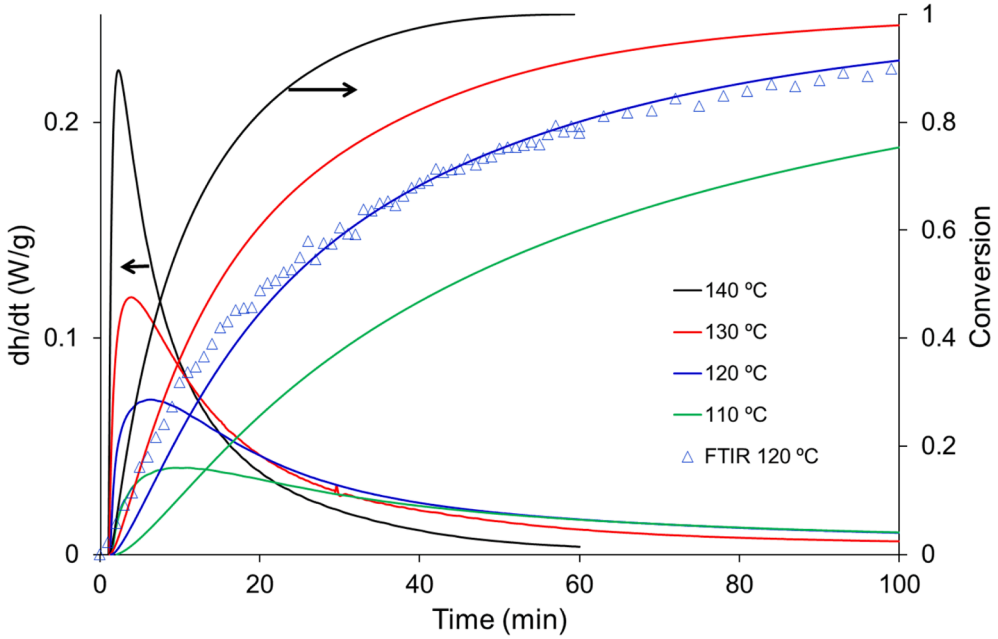

Fig. 3. Isothermal curing profiles corresponding to the thermal (stage 2) curing of Base-3D at different temperatures. The samples were previously photocured at 30 °C.

$$\ln t_{i,\alpha} = \ln\left(\frac{g(\alpha)}{A_\alpha}\right) + \frac{E_\alpha}{R{\cdot}T_i} \quad (1)$$

where A_α is the pre-exponential factor, E_α is the activation energy and $t_{i,\alpha}$ the time required to achieve a fixed conversion at temperature T_i and $g(\alpha)$ is the integral model function defined as.

$$g(\alpha) = \int_0^\alpha \frac{d\alpha}{f(\alpha)} \quad (2)$$

where $f(\alpha)$ is the differential model function. If the separable function assumption is correct, a plot of $\ln t_{i,\alpha}$ versus $(R{\cdot}T_i)^{-1}{}_i$, gives a straight with slope E_α and y-intercept $\ln(g(\alpha)/A_\alpha)$. If the the model function ($g(\alpha)$ or $f(\alpha)$ is known, the pre-exponential factor can easily be calculated for each conversion. To validate the model, equation (1) is rearranged to give.

$$\ln\left(\frac{t_{i,\alpha}}{g(\alpha)}\right) = -\ln(A) + \frac{E}{R{\cdot}T_i} \quad (3)$$

Plotting $\ln(t_{i,\alpha}/g(\alpha))$ against $(R{\cdot}T_i)^{-1}$ for all conversions will yield a straight line with a slope E, and y-intercept –ln(A) if the kinetic model is correct.

The Kamal model function and its integral are given in equations (4) and (5), respectively.

$$f(\alpha) = \alpha^m(1-\alpha)^n \quad (4)$$

$$g(\alpha) = \frac{1}{1-m}\left(\frac{\alpha}{1-\alpha}\right)^{1-m} \quad (5)$$

As mentioned previously, it is assumed that $n + m = 2$, where n and m are the partial reaction orders. In our analysis, the parameters n and m were calculated using the GRG Nonlinear algorithm of MS Excel. The algorithm attempts to maximize the R-squared value of the linear regression which also gives the activation energy E and the logarithm of the pre-exponential factor A (vide supra). The resulting kinetic parameters are tabulated in Table 2. The values of E were practically identical to the apparent activation energy obtained using the isoconversional integral method. It can also be observed that the activation energies and reaction orders are very similar for all formulations. This indicates that the epoxy-acid reaction proceeds via the same mechanism regardless of other formulation components and the employed catalyst. The most noticeable difference is the value of the pre-exponential factor and the calculated kinetic constant at 120 °C. The fastest curing system is Base-MI. When $Zn(AcAc)_2$ is used as catalyst, the curing reaction slows down. Accordingly, both Base-Zn and Base-3D have slow and comparable curing kinetics. This difference in reactivity is also illustrated in Fig. 4. It can be seen that the effect of PEGMA in the Base 3D formulation is practically insignificant since complete conversion is attained in about 3 h regardless of the presence of PEGMA.

The interpretation of the kinetic parameters is not straightforward due to the fact that in autocatalytic curing reactions, E and A tend to compensate each other. As a result, referring to either parameter alone would be misleading in drawing conclusions about reaction rate. However, the rate constant k, being a combination of the two, represents curing kinetics in a more reliable way [30]. Corroborating what was observed experimentally, the rate constant at 120 °C ($k_{120^\circ c}$) of 1-MI containing formulations (Base-Mix and Base-MI) are higher than those of $Zn(AcAc)_2$ containing formulations (Base-Zn and Base-3D) by an order of magnitude. Regarding reaction orders, the values are comparable across different formulations, suggesting a single, catalyst-independent curing mechanism. Nevertheless, as will be shown later, the choice of catalyst brings about a trade-off between the rate of curing and the rate of relaxation (vide infra).

Table 2
Kinetic parameters obtained by model-fitting and autocatalytic model function. $\boldsymbol{k_{120^\circ c}}$ was calculated using Arrhenius eqn.

Formulation	n	m	$E(kJ/mol)$	$lnA(min^{(-1)})$	$k_{120^\circ C}(min^{-1})$
Base-Zn	1.75	0.25	71	19.02	0,0671
Base-Mix	1.76	0.24	72	20.75	0,2787
Base-MI	1.68	0.32	73	21.41	0,3972
Base-3D	1.65	0.35	72	19.26	0,0628

The results of the kinetics analysis suggest also that the storage stability of the prepared formulations and the intermediate stage material would be much higher in the case of the formulations containing only $Zn(AcAc)_2$. The time t needed to reach a 5 % conversion at 30 °C was extrapolated making use of the kinetic parameters in Table 2 and expression $g(\alpha) = k{\cdot}t$, where $k = A{\cdot}exp(-E/RT)$ is the rate constant. For the Base-3D formulation, the estimated time was 42 h, and for Base-Mix it was less than 6 h. Therefore, it can be projected that using $Zn(AcAc)_2$ would guarantee sufficient storage stability. For experimental verification of this, intermediate stage materials were kept in storage at 30 °C for prolonged periods to check their stability. The samples were periodically tested in DSC to monitor the evolution of T_g and residual heats. As can be seen in Fig. 5, the presence of 1-MI jeopardizes the storage stability, as the T_g increases from −27 °C to −12 °C in only 2 days (T_g reading on day 2 is marked with blue dashed line in Fig. 5), while the residual heat drops by 46%. The T_g reaches 28 °C in about one month. On the other hand, when $Zn(AcAc)_2$ is the catalyst, storage stability is remarkable. The increase in T_g is below 10 °C even after 10 days. In spite of the inherent extrapolation error, the kinetic model predictions are in reasonable agreement with experimental findings.

In spite of the good storage stability of its formulations, the solubility of $Zn(AcAc)_2$ can be a matter of concern. Compatibilization of zinc salts might be complicated unless there is sufficient concentration of hydroxyls and/or carboxyls in the medium to facilitate desirable ionic interactions. As stated previously, even though the formulations herein prepared have high hydroxyl and carboxyl contents, slightly turbid solutions were obtained when $Zn(AcAc)_2$ was used. In contrast, the 1-MI catalyst, being in liquid form, was much easily dissolved during preparation of formulations. Nevertheless, the lower storage stability of its formulations is a caveat.

3.2. Thermomechanical properties

Table 3 summarizes glass transition temperatures T_g of the materials at the two curing stages, as well as after further thermal treatment at 180 °C for 4 h, which was done to ensure that transesterification reactions attained equilibrium. Similar thermal treatment procedures were employed by other researchers as well [12,31].

The choice of catalyst did not seem to alter the T_g at any curing stage. However, the modification by PEGMA seems to have slightly decreased T_g at all stages, possibly due to a decrease in crosslinking density along with an increase in free volume caused by the presence of the aliphatic side chain of PEGMA. The thermal post-treatment seems to have a beneficial effect in terms of T_g, especially in PEGMA-free formulations. As will be shown later, at 180 °C, transesterification occurs at rapid rates, giving way to new structural fragments containing beta-hydroxy esters, diols, and diesters. As will be shown, the overall network connectivity appears to increase as a result of these new structures. It was seen that treatments longer than 4 h did not increase T_g any further (vide infra). Fully cured samples (without post-treatment) were analyzed in DMA and results are given in Fig. 6. Although there was no visual difference between Base-3D and the rest of the (PEGMA-free) formulations, the PEGMA-free samples exhibited bimodal tan delta curves regardless of the catalyst used. In spite of the acrylate/methacrylate and the epoxy-acid interconnection (facilitated by the coupling agent GMA), the overall network appears to have a heterogeneous structure, possibly due to the tightly crosslinked polyacrylate network impeding the homogeneous penetration of the epoxy-acid network into it. The narrow tan

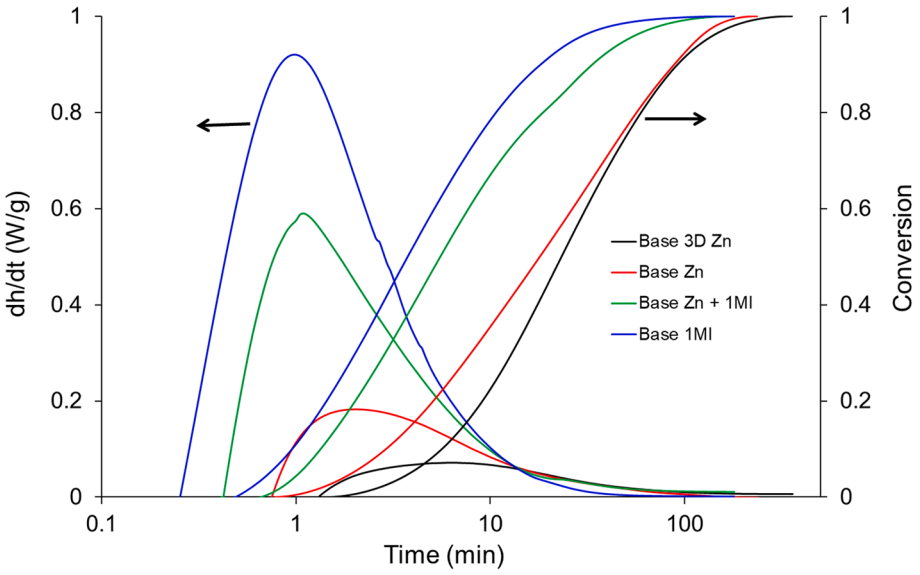

Fig. 4. Isothermal DSC heat flow and conversion curves of all formulations at 120 °C.

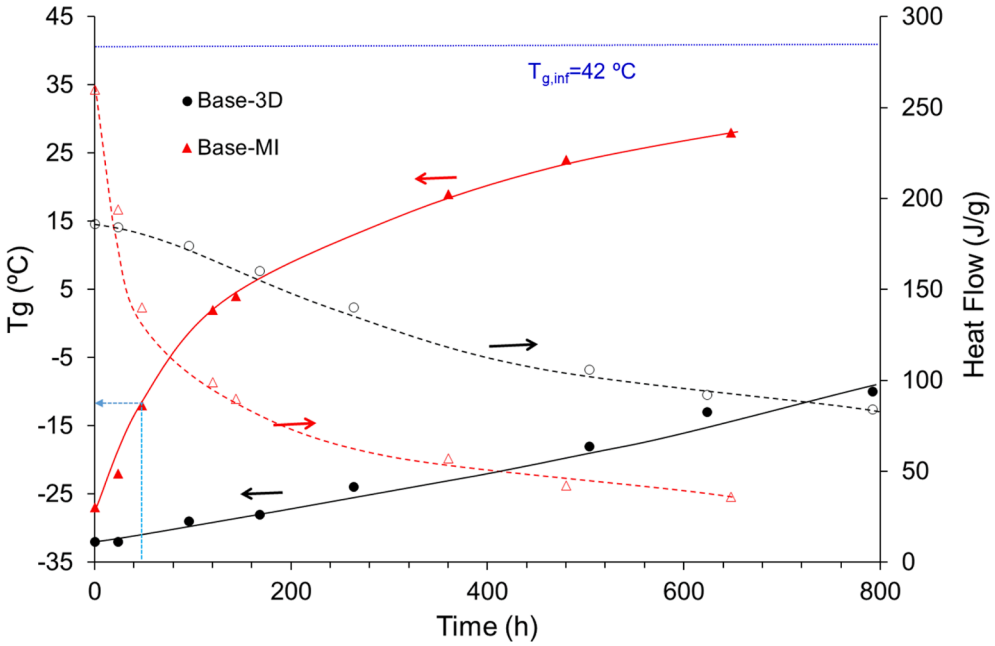

Fig. 5. DSC measured residual curing heats (hollow symbols) and T_g of intermediate materials (filled symbols) showing the effect of catalyst on storage stability. A temperature ramp of 10 °C min-1 was used in heat scans to determine residual heats. T_g reading on day 2 is marked with blue dashed arrow. (For interpretation of the references to colour in this figure legend, the reader is referred to the web version of this article.)

Table 3
Tg of formulations at different stages of cure/processing. Materials attain stage 1 (S1) after being photocured at 30 °C, stage 2 (S2) after thermal cure at 120 °C for 12 h, and final stage after thermal post-treatment at 180C for 4 h.

Formulation	$T_{g,S1}(^{\circ}C)$	$T_{g,S2}(^{\circ}C)$	$T_{g,final}(^{\circ}C)$
Base-Zn	−25	43	52
Base-MI	−28	42	50
Base-Mix	−27	43	51
Base-3D	−30	41	46

delta peak at lower temperature would correspond to the epoxy-rich fraction (analysis of neat ER-GLU epoxy-acid polymer produced a T_g of ca. 50 °C measured with DSC), while the second and broader peak should be due to the acrylate homopolymer phase (pure GLYDA polymer has a calorimetric T_g of 85 °C, which would correspond to a tan delta peak around 100–110 °C). Similar effects were reported in other dual-cured acrylate/epoxy-anhydride 3D-printable formulations [27,28], The Base-3D material exhibited a narrower relaxation, possibly due to a more homogeneous, less tightly cross-linked acrylate network facilitated by PEGMA.

The effect of thermal post-treatment on viscoelastic properties was investigated for Base-3D. As can be seen in Fig. 7, a slight increase in tan delta peak, along with an increase in rubbery plateau (E') is observed during the first 2 h due to the network rearrangement caused by the transesterification. When 1-MI was used as catalyst, a post-treatment of up to 4 h was required in order to obtain a stable structure, which suggests that $Zn(AcAc)_2$ is a more effective catalyst for the

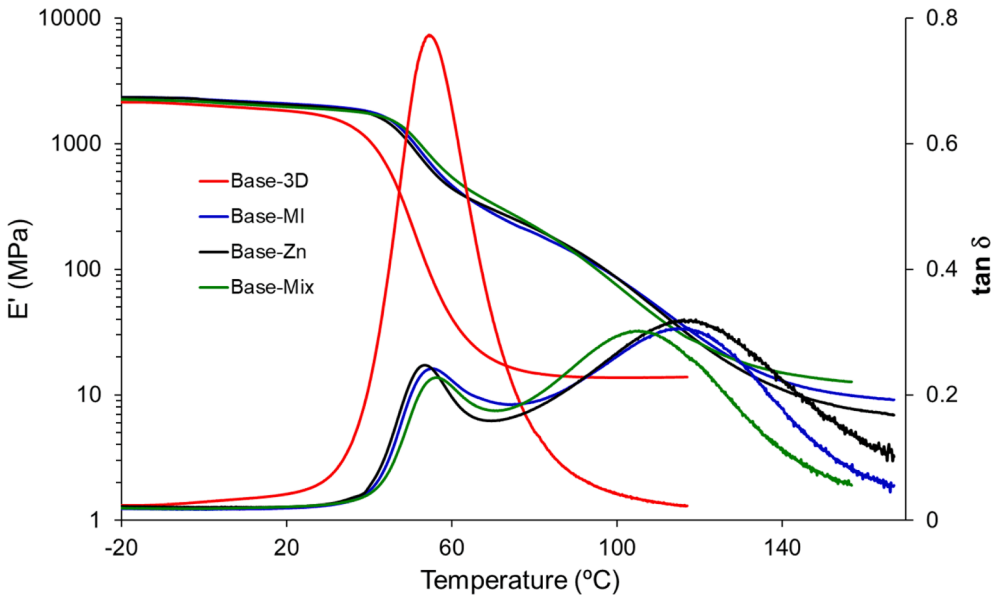

Fig. 6. Storage moduli (*E'*) and tan delta curves of all formulations at curing stage 2.

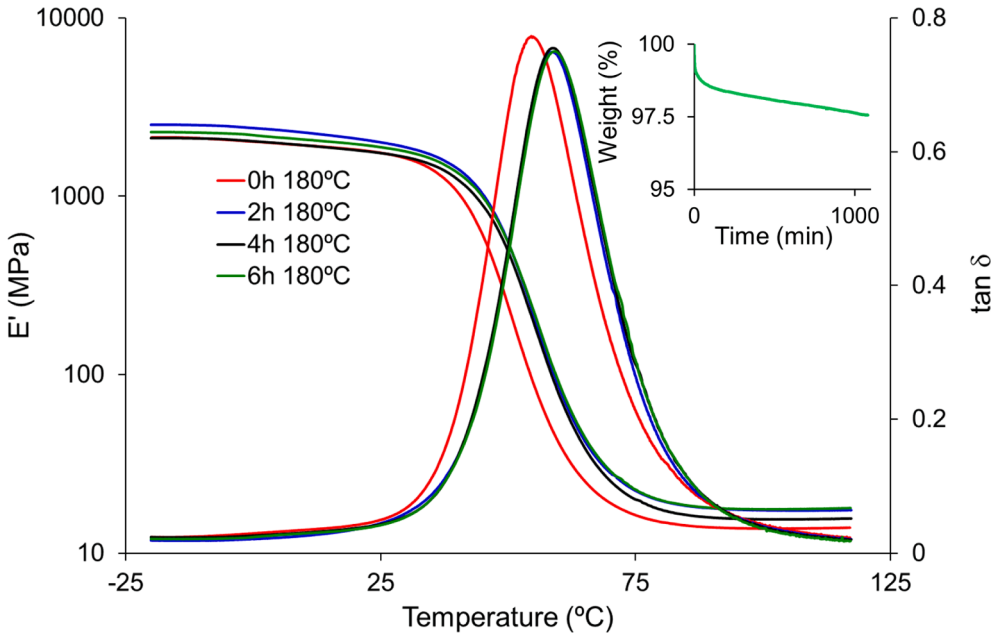

Fig. 7. Effect of thermal post-treatment (at 180 °C) on viscoelastic behavior of Base-3D. Inset: TGA curve at 180 °C. No significant weight loss is observed in 24 h.

transesterification. In the light of these findings, a post-treatment duration of 4 h is established for all samples studied. The material showed no significant thermal degradation at the post-treatment temperature of 180 °C (Fig. 7 inset).

3.3. Bond exchange mechanisms

The fully cured polyacrylate-epoxy dual network can undergo transesterification reactions in a number of ways, some of which are depicted in Scheme 2. An exhaustive scheme depicting all possible transesterifications is not provided due to space restrictions. These ester-hydroxyl exchanges can take place in any arbitrary combination involving the β-hydroxy esters in i) the poly(acrylate), ii) the GMA-GLU oligomer, and iii) the epoxy-acid (ER-GLU) polymer,

As can be seen from Scheme 2, overall network connectivity can be altered as the reactions progress until reaching equilibrium. The mobility of the network is slightly more restricted in the equilibrium configuration, as was suggested by the shift of tan delta during the first 2 h of thermal post-treatment (see Fig. 7).

3.4. Stress relaxation behavior

Fig. 8 shows the effect of the thermal post-treatment on the relaxation of Base-3D fully cured material at 180 °C. In post-treated samples, relaxation is slowed down slightly due to a more densely cross-linked structure after transesterification equilibrium is established (Fig. 7). As observed before, 2 h are sufficient to reach an equilibrium structure and repeatable relaxation kinetics are observed after 2 h of thermal post treatment.

Fig. 9 shows the effect of temperature on the stress relaxation of post-

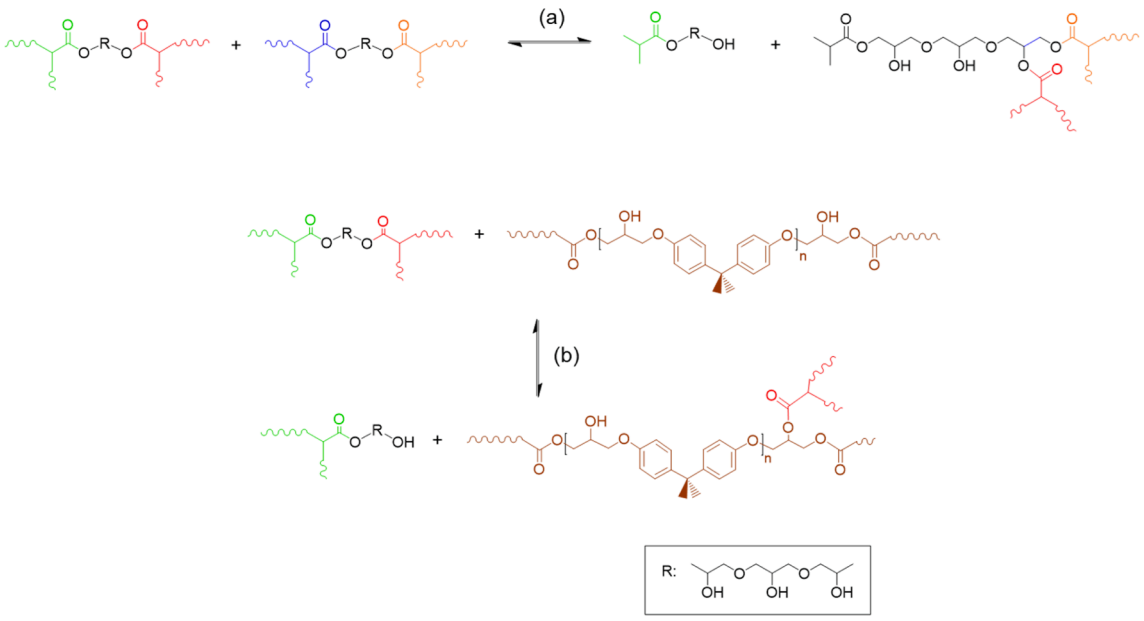

Scheme 2. Possible ester-hydroxyl exchange reactions within the polyacrylate network (a) and in between polyacrylate and epoxy-acid networks (b).

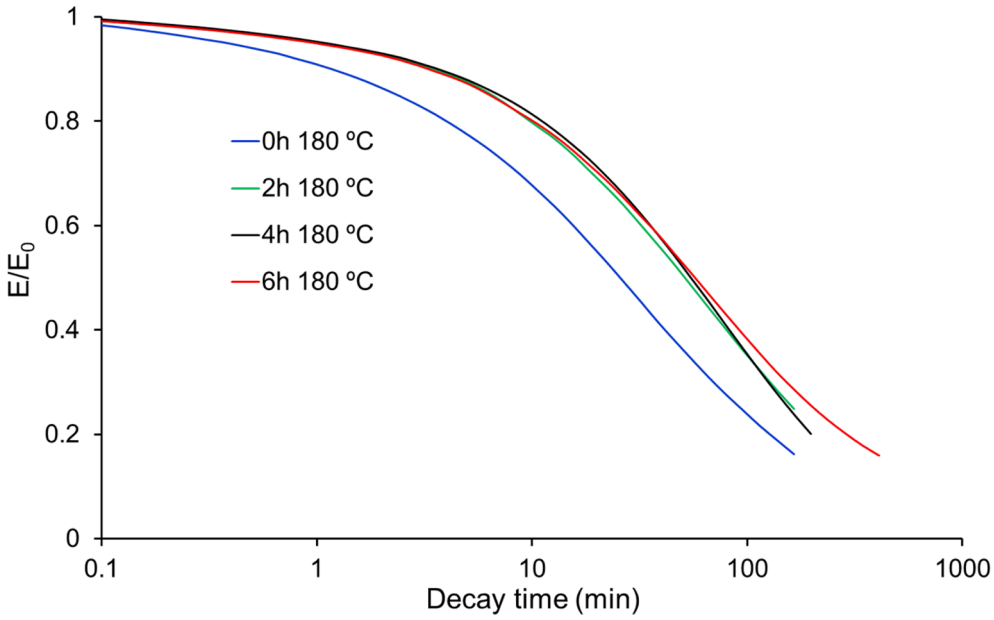

Fig. 8. Stress relaxation of Base-3D post-treated for different times. Specimens were subjected to a strain of 1% in 3-point bending.

treated Base-3D samples. Relaxation profiles evidence that transesterification hastens as temperature is increased: While at 160 °C full stress relaxation requires more than one day, at 200 °C it is nearly complete in 2 h. These results compare well with other transesterification-based CANs reported in the literature [12,16].

Naturally, the choice of catalyst also affects stress relaxation behavior, as seen in Fig. 10. When 1-MI was used as co-catalyst, relaxation rate slowed down by a factor of 2 to 3, and when 1-MI was used singularly, transesterification rate decreased by a decade. The presence of PEGMA did not seem to have any detrimental effect on the relaxation kinetics.

The poor relaxtion behavior of the 1-MI catalyzed formulation was surprising, since 1-MI is documented as an excellent transesterification catalyst [25]. The effect observed herein was rationalized in terms of the network structure and the role of 1-MI in the epoxy-acid reaction. (1)-MI is known to have nucleophilic behavior, forming adducts and complexes with the epoxide component which in turn propagate the curing [32,33]. In our hybrid system, the epoxy-acid reaction is the second curing reaction that takes place within the polyacrylate matrix formed earlier. As a consequence, a significant fraction of 1-MI may be covalently bound to the polyester network structure formed by the reaction between ER (and GMA) and GLU. As suggested by the bimodal glass transitions seen in Fig. 6 (except Base-3D), the hybrid network is not entirely homogeneous. Consequently, one can argue that the part of 1-MI segregated in the epoxy-acid network would be unavailable to catalyze the transesterifications involving the β-hydroxy esters of the polyacrylate network. On the other hand, $Zn(AcAc)_2$ would be homogeneously distributed within the material and would have no preferred interaction within a particular region of the network, therefore maintaining its availability to catalyze both intra- and inter-network

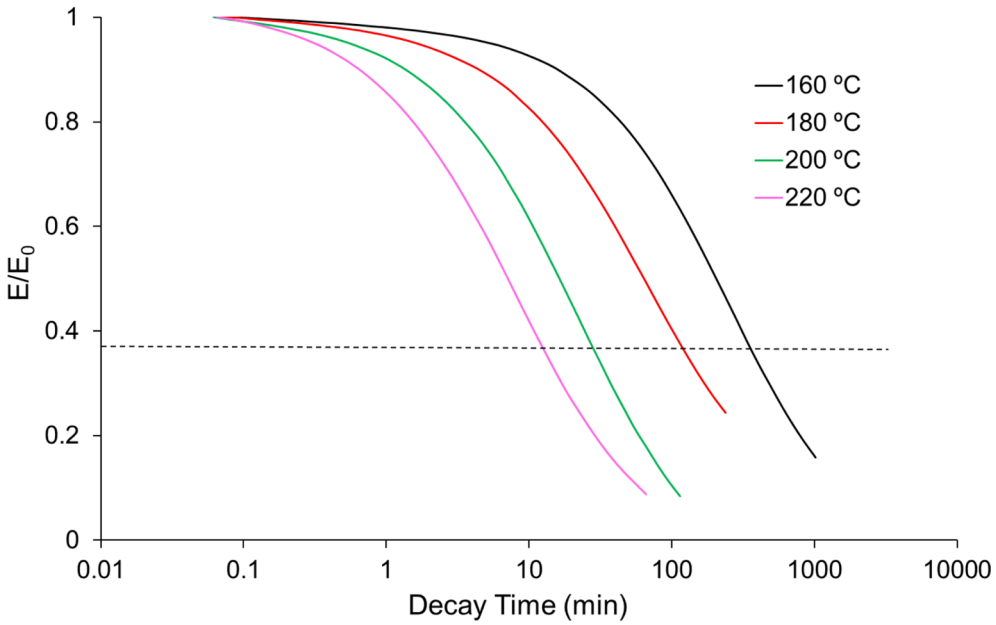

Fig. 9. Normalized stress relaxation curves of Base-3D at varying temperatures. The dashed line marks the E/E_0 value of 1/e (i.e. at ~63% of complete relaxation) used to calculate the vitrimeric transition temperature T_v.

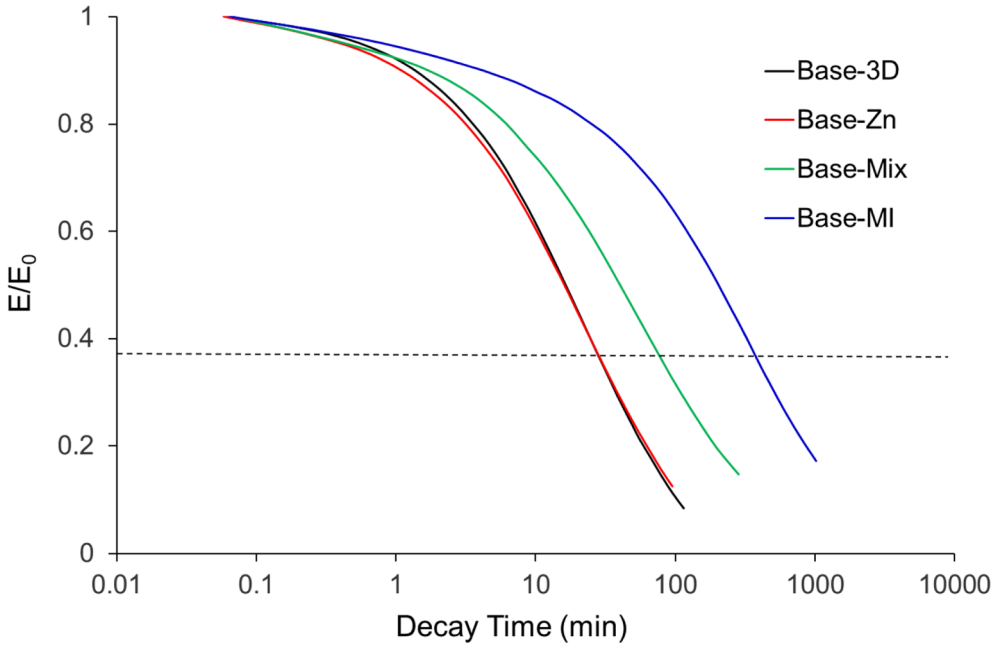

Fig. 10. Stress relaxation of all formulations at 200 °C, samples were post-treated for 4 h at 180 °C prior to analysis.

transesterifications. In Base-Mix, 1-MI may have had an acid-base interaction with $Zn(AcAc)_2$, thereby neutralizing it partially, leading to slower relaxation in comparison with the material containing only $Zn(AcAc)_2$ as catalyst.

To elaborate on relaxation kinetics, each formulation was tested at four different temperatures to confirm Arrhenius-like behavior of the characteristic relaxation times τ^* (i.e. time required to relax ~63% of the stress) which is expressed as $\tau(T) = \tau_0 \cdot \exp(E_{act}/RT)$. As Base-MI material exhibits longer relaxation times compared to other formulations, it was tested at higher temperatures. The Arrhenius plots of the relaxation times are shown in Fig. 11. The test temperatures are specified in the figure caption. As can be deduced from the slope of the different lines, the activation energies of the different systems are similar, regardless of the network structure and the catalyst employed. The calculated values, shown in Table 4, are comparable to other transesterification-based CANs reported in literature [7,12,24].

The so-called liquid-to-solid transition temperature, T_v was determined for each formulation following the procedure outlined by Capelot et al [24]. The T_v is defined as the temperature at which the viscosity exceeds 10^{12} Pa.s. Below this temperature, transesterification rate is assumed negligible. Applying the Maxwell equation given as $\eta = G \cdot \tau^*$ together with the relation between shear modulus and tensile modulus $G = E^{'}/[2(1+\nu)]$ where ν is the Poisson's ratio that attains a value of 0.5 in the rubbery state, we get $G = E^{'}/3$. Taking $E^{'}$ 3 MPa, τ^* is calculated as 10^6 s. Using this result, it is straightforward to determine T_v from the plots in Fig. 11. It is evidenced from the graph that the T_v of Base-MI is

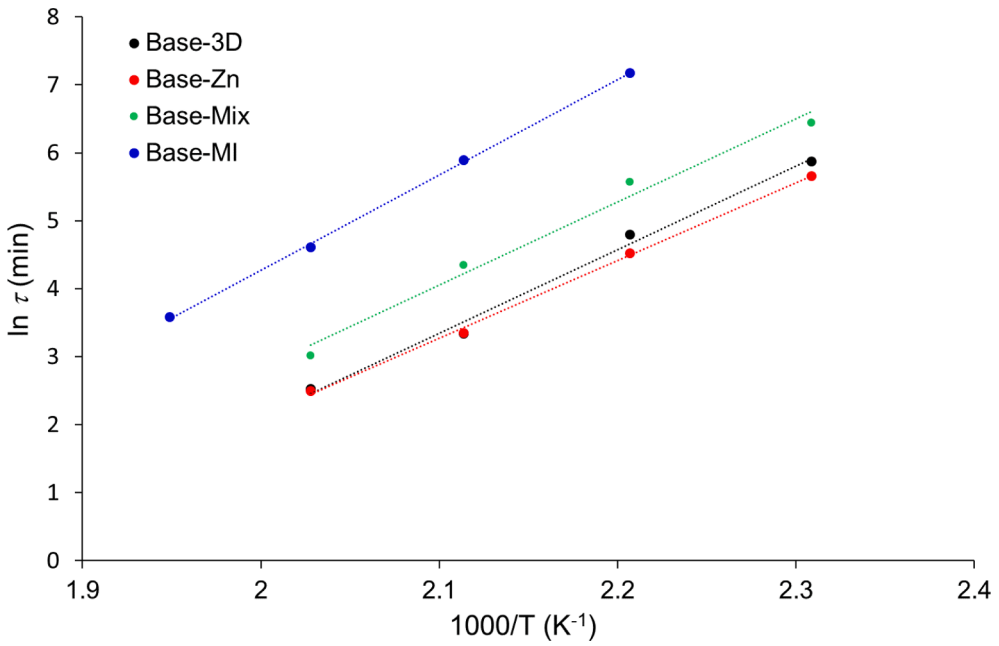

Fig. 11. Arrhenius plots of the relaxation times. Base-Zn, Base-Mix and Base-3D were tested at 160, 180, 200 and 220 °C whereas Base-MI was tested at 180, 200, 220 and 240 °C.

Table 4
Calculated E_{act} and T_v of the different formulations, obtained from analysis of samples post-treated at 180 °C for 4 h.

Formulation	$E_{act}(kJ/mol)$	$T_v(°C)$
Base-Zn	94.8	133
Base-MI	116.8	177
Base-Mix	101.7	148
Base-3D	102.2	138

significantly higher than others. Indeed, below 180 °C, Base-MI did not relax within a practical timeframe. Actually, the T_v of Base-MI suggests its relaxation rate would be negligible below 180 °C, while relaxation would occur for Base-Zn and Base-3D at temperatures as low as 140 °C. All these observations corroborate experimental findings presented previously.

3.5. Printed, repaired and recycled materials

Complex objects can be DLP-printed easily and at rapid rates with Base-3D. Photographs of two such objects are given as inset in Fig. 12. To test repairability, rectangular DMA samples were 3D printed using Base-3D with the same dimensions as in earlier stress–strain tests. One of these samples were printed with a hole at its center as can be seen in the legend of Fig. 12. This perforated sample exhibited a significantly lower Young's modulus (846 MPa) compared to the pristine sample (1323 MPa). Later, it was repaired by simply filling the hole with either the liquid Base-3D, or a commercial acrylic resin with trade name Spot-LV (Spot-A Materials, Barcelona, Spain) which has a similar final T_g but has no bond exchanging components (i.e. a CAN-free material). Both repaired samples were fully processed using the established procedure (i.e. Photocure -> thermal cure –> thermal post-treatment). Whereas the stress-response of the sample repaired using Base-3D indicated full recovery, the sample repaired using Spot-LV exhibited only partial recovery. The recycled sample exhibited a Young's modulus of 1514 MPa, a value slightly higher than that of the original sample (1323 MPa) probably due to volatilization of small fragments during the recycling process.

Recyclability was tested on DMA samples. Fully cured samples were

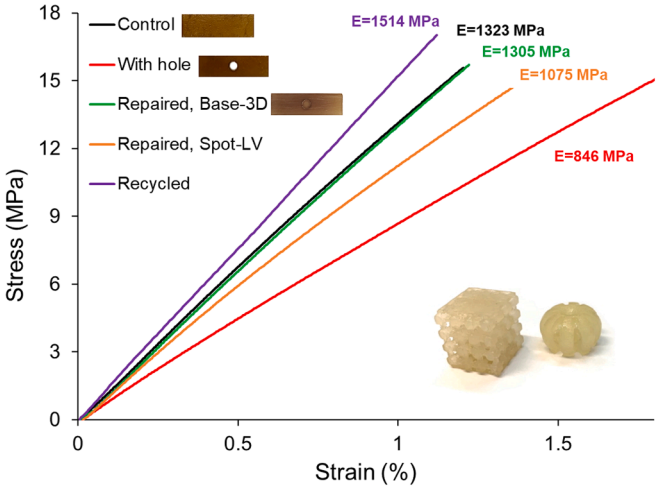

Fig. 12. Stress-strain plots of fully cured Base-3D samples. Inset: A zeolite structure and a model fountain printed with Base-3D.

finely chopped and later hot-pressed as explained in Materials and Methods section. From the solid films obtained, new DMA samples were die-cut in the same dimensions, after which they were analyzed in DMA at the same conditions. As seen in Fig. 13, apart from a slight increase in storage modulus and a slight decrease of rubbery plateau, both of which are practically insignificant, the recycled material is identical to its pristine counterpart. The inset in Fig. 13 illustrates the recycling procedure.

4. Conclusions

We have described a new poly(hydroxy-ester) dynamic network obtained through a simple dual-cure procedure. The unique formulation combines a photocurable diacrylate already rich in β-hydroxy esters and hydroxyls, with an acid cured epoxy to yield a hybrid network capable of undergoing intra- and inter-network transesterifications. This is exploited in repairing and recycling these vitrimeric materials via facile

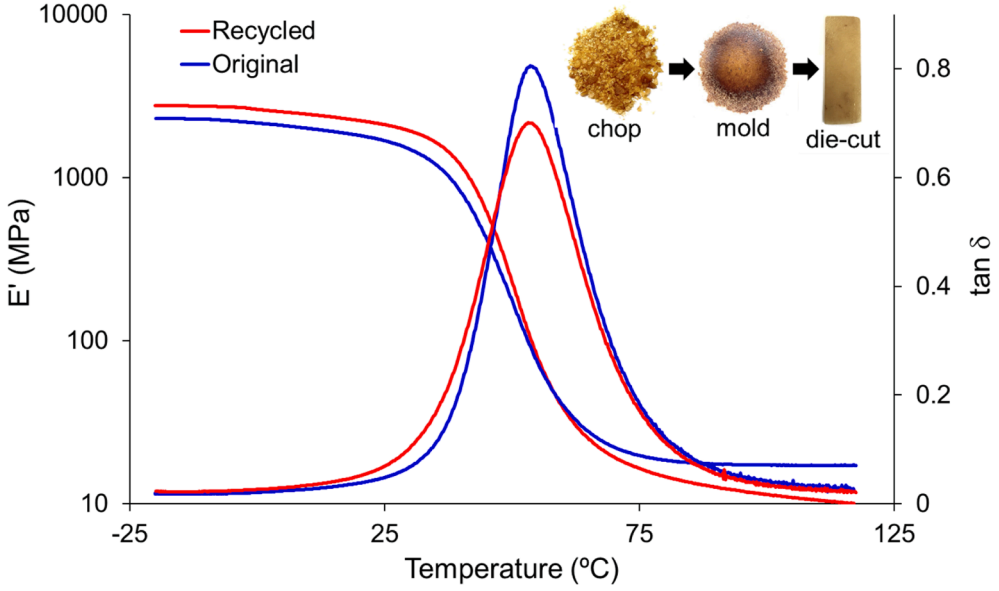

Fig. 13. DMA storage modulus and tan delta curves of recycled samples in comparison with a pristine one. The recycling procedure is depicted as inset.

procedures.

Zinc acetylacetonate and 1-methylimidazole were tested as catalysts both of the epoxy-acid reaction and transesterifications. At moderately elevated temperatures, transesterification reactions are initiated across the hybrid network at sufficiently high rates. Reaction equilibrium is reached in a few hours, which brings about an apparent increase in crosslinking density and T_g. When subjected to strain, these materials are able to relax their stress within practical timeframes at temperatures as low as 140 °C. Their relaxation kinetics were comparable to other vitrimers based on transesterification reactions.

The imidazole catalyst was more efficient in the catalysis of the epoxy-acid reaction but showed a poor performance as transesterification catalyst. The epoxy-acid reaction was not as fast when the zinc catalyst was used, but it reached completion in a reasonable time. This lower reactivity made the zinc catalyst more adequate in terms of storage stability of the uncured formulations and intermediate stage materials. Moreover, the transesterification was significantly faster with the zinc catalyst. A combination of the two catalysts produced an intermediate effect, promoting fast epoxy-acid reaction while retaining an acceptable rate of transesterification.

The formulation modified with PEGMA, thanks to its low viscosity, could be used to print objects in a DLP type 3D printer. After thermal curing and thermal post-treatment, the resulting fully-cured 3D-printed objects were shown to be repairable and completely recyclable. By combining processing flexibility of dual-cure formulations with the versatility of DLP-based 3D printing methods, these novel formulations show promise in advanced applications requiring tailor-made properties and processing flexibility. Coupled with their repair and recycle capabilities facilitated by a covalently adaptable network structure, they can potentially replace conventional thermosets and reduce their carbon footprint.

CRediT authorship contribution statement

J. Casado: Formal analysis, Investigation, Writing – original draft. **O. Konuray:** Conceptualization, Investigation, Methodology, Supervision, Validation, Writing – original draft, Writing – review & editing. **A. Roig:** . **X. Fernandez-Francos:** Conceptualization, Methodology, Supervision, Validation, Writing – review & editing. **X. Ramis:** Conceptualization, Formal analysis, Funding acquisition, Investigation, Methodology, Project administration, Resources, Supervision, Validation, Writing – review & editing.

Declaration of Competing Interest

The authors declare that they have no known competing financial interests or personal relationships that could have appeared to influence the work reported in this paper.

Acknowledgements

The authors acknowledge the funding sources disclosed below. The authors also thank Po.Int.Er S.R.L. for supplying the epoxy resin. X. Fernández-Francos and O. Konuray acknowledge the Serra-Húnter programme (Generalitat de Catalunya).

Funding

This work was funded by the Spanish Ministry of Science and Innovation (MCNI/AEI) through R&D projects PID2020-115102RB-C21 and PID2020-115102RB-C22, and also by Generalitat de Catalunya (2017-SGR-77 and BASE3D).

Data availability

The raw data required to reproduce these findings are available upon request from authors.

References

[1] C.J. Kloxin, T.F. Scott, B.J. Adzima, C.N. Bowman, Covalent adaptable networks (CANs): A unique paradigm in cross-linked polymers, Macromolecules 43 (2010) 2643–2653, https://doi.org/10.1021/ma902596s.
[2] W. Denissen, J.M. Winne, F.E. Du Prez, Vitrimers: permanent organic networks with glass-like fluidity, Chem. Sci. 7 (2016) 30–38, https://doi.org/10.1039/C5SC02223A.
[3] C.J. Kloxin, C.N. Bowman, Covalent adaptable networks: Smart, reconfigurable and responsive network systems, Chem. Soc. Rev. 42 (2013) 7161–7173, https://doi.org/10.1039/c3cs60046g.
[4] W. Zou, J. Dong, Y. Luo, Q. Zhao, T. Xie, Dynamic Covalent Polymer Networks: from Old Chemistry to Modern Day Innovations, Adv. Mater. 29 (2017) 1–18, https://doi.org/10.1002/adma.201606100.
[5] B. Krishnakumar, R.V.S.P. Sanka, W.H. Binder, V. Parthasarthy, S. Rana, N. Karak, Vitrimers: Associative dynamic covalent adaptive networks in thermoset polymers, Chem. Eng. J. 385 (2020), 123820, https://doi.org/10.1016/j.cej.2019.123820.
[6] M. Podgórski, B.D. Fairbanks, B.E. Kirkpatrick, M. McBride, A. Martinez, A. Dobson, N.J. Bongiardina, C.N. Bowman, Toward Stimuli-Responsive Dynamic Thermosets through Continuous Development and Improvements in Covalent

Adaptable Networks (CANs), Adv. Mater. 32 (2020) 1–26, https://doi.org/10.1002/adma.201906876.
[7] D. Montarnal, M. Capelot, F. Tournilhac, L. Leibler, Silica-Like Malleable Materials from Permanent Organic Networks, Science 334 (6058) (2011) 965–968.
[8] K. Yu, P. Taynton, W. Zhang, M.L. Dunn, H.J. Qi, Reprocessing and recycling of thermosetting polymers based on bond exchange reactions, RSC Adv. 4 (2014) 10108–10117, https://doi.org/10.1039/c3ra47438k.
[9] X. Niu, F. Wang, X. Kui, R. Zhang, X. Wang, X. Li, T. Chen, P. Sun, A.C. Shi, Dual Cross-linked Vinyl Vitrimer with Efficient Self-Catalysis Achieving Triple-Shape-Memory Properties, Macromol. Rapid Commun. 40 (2019) 1–8, https://doi.org/10.1002/marc.201900313.
[10] M. Capelot, D. Montarnal, F. Tournilhac, L. Leibler, Metal-catalyzed transesterification for healing and assembling of thermosets, J. Am. Chem. Soc. 134 (2012) 7664–7667, https://doi.org/10.1021/ja302894k.
[11] L. Imbernon, S. Norvez, L. Leibler, Stress Relaxation and Self-Adhesion of Rubbers with Exchangeable Links, Macromolecules 49 (2016) 2172–2178, https://doi.org/10.1021/acs.macromol.5b02751.
[12] B. Zhang, K. Kowsari, A. Serjouei, M.L. Dunn, Q. Ge, Reprocessable thermosets for sustainable three-dimensional printing, Nat. Commun. 9 (2018), https://doi.org/10.1038/s41467-018-04292-8.
[13] C. Taplan, M. Guerre, F.E. Du Prez, Covalent Adaptable Networks Using β-Amino Esters as Thermally Reversible Building Blocks, J. Am. Chem. Soc. 143 (2021) 9140–9150, https://doi.org/10.1021/jacs.1c03316.
[14] F. Cuminet, S. Caillol, É. Dantras, É. Leclerc, V. Ladmiral, Neighboring Group Participation and Internal Catalysis Effects on Exchangeable Covalent Bonds: Application to the Thriving Field of Vitrimer Chemistry, Macromolecules 54 (2021) 3927–3961, https://doi.org/10.1021/acs.macromol.0c02706.
[15] J. Han, T. Liu, C. Hao, S. Zhang, B. Guo, J. Zhang, A Catalyst-Free Epoxy Vitrimer System Based on Multifunctional Hyperbranched Polymer, Macromolecules 51 (2018) 6789–6799, https://doi.org/10.1021/acs.macromol.8b01424.
[16] E. Rossegger, R. Höller, D. Reisinger, M. Fleisch, J. Strasser, V. Wieser, T. Griesser, S. Schlögl, High resolution additive manufacturing with acrylate based vitrimers using organic phosphates as transesterification catalyst, Polymer 221 (2021), https://doi.org/10.1016/j.polymer.2021.123631.
[17] U. Shaukat, E. Rossegger, S. Schlögl, Thiol–acrylate based vitrimers: From their structure–property relationship to the additive manufacturing of self-healable soft active devices, Polymer 231 (2021) 29–34, https://doi.org/10.1016/j.polymer.2021.124110.
[18] E. Rossegger, R. Höller, D. Reisinger, J. Strasser, M. Fleisch, T. Griesser, S. Schlögl, Digital light processing 3D printing with thiol-Acrylate vitrimers, Polym. Chem. 12 (2021) 638–644, https://doi.org/10.1039/d0py01520b.
[19] Q. Shi, K. Yu, X. Kuang, X. Mu, C.K. Dunn, M.L. Dunn, T. Wang, H. Jerry Qi, Recyclable 3D printing of vitrimer epoxy, Mater. Horizons. 4 (2017) 598–607, https://doi.org/10.1039/c7mh00043j.
[20] Z. Chen, M. Yang, M. Ji, X. Kuang, H.J. Qi, T. Wang, Recyclable thermosetting polymers for digital light processing 3D printing, Mater. Des. 197 (2021) 189, https://doi.org/10.1016/j.matdes.2020.109189.
[21] C. Lu, C. Wang, J. Yu, J. Wang, F. Chu, Two-Step 3 D-Printing Approach toward Sustainable, Repairable, Fluorescent Shape-Memory Thermosets Derived from Cellulose and Rosin, ChemSusChem 13 (2020) 893–902, https://doi.org/10.1002/cssc.201902191.
[22] X. Fernández-francos, O. Konuray, X. Ramis, À. Serra, S. De, Enhancement of 3D-printable materials by dual-curing procedures, Materials. 14 (2021) 1–23.
[23] O. Konuray, X. Fernández-Francos, X. Ramis, À. Serra, State of the Art in Dual-Curing Acrylate Systems, Polymers. 10 (2018) 178, https://doi.org/10.3390/polym10020178.
[24] M. Capelot, M.M. Unterlass, F. Tournilhac, L. Leibler, Catalytic control of the vitrimer glass transition, ACS Macro Lett. 1 (2012) 789–792, https://doi.org/10.1021/mz300239f.
[25] F.I. Altuna, C.E. Hoppe, R.J.J. Williams, Shape memory epoxy vitrimers based on DGEBA crosslinked with dicarboxylic acids and their blends with citric acid, RSC Adv. 6 (2016) 88647–88655, https://doi.org/10.1039/c6ra18010h.
[26] X. Fernández-Francos, S.G. Kazarian, X. Ramis, À. Serra, Simultaneous Monitoring of Curing Shrinkage and Degree of Cure of Thermosets by Attenuated Total Reflection Fourier Transform Infrared (ATR FT-IR) Spectroscopy, Appl. Spectrosc. 67 (2013) 1427–1436, https://doi.org/10.1366/13-07169.
[27] O. Konuray, A. Altet, J. Bonada, A. Tercjak, X. Fernández-francos, X. Ramis, Epoxy Doped, Nano-scale Phase-separated Poly-Acrylates with Potential in 3D Printing, Macromol. Mater. Eng. 2000558 (2021) 1–10, https://doi.org/10.1002/mame.202000558.
[28] O. Konuray, A. Sola, J. Bonada, A. Tercjak, A. Fabregat-Sanjuan, X. Fernández-Francos, X. Ramis, Cost-Effectively 3D-Printed Rigid and Versatile Interpenetrating Polymer Networks, Materials. 14 (16) (2021) 4544.
[29] M. Morancho, X. Fernández-Francos, X. Ramis, Curing kinetics of dually-processed acrylate-epoxy 3D printing resins, Thermochim. Acta. 701 (2021), https://doi.org/10.1016/j.tca.2021.178963.
[30] S. Vyazovkin, C.A. Wight, KINETICS IN SOLIDS, Annu. Rev. Phys. Chem. 48 (1997) 125–149, https://doi.org/10.1146/annurev.physchem.48.1.125.
[31] F.I. Altuna, C.E. Hoppe, R.J.J. Williams, Epoxy vitrimers: The effect of transesterification reactions on the network structure, Polymers. 10 (2018), https://doi.org/10.3390/polym10010043.
[32] M. Pire, C. Lorthioir, E.K. Oikonomou, S. Norvez, I. Iliopoulos, B. Le Rossignol, L. Leibler, Imidazole-accelerated crosslinking of epoxidized natural rubber by dicarboxylic acids: A mechanistic investigation using NMR spectroscopy, Polym. Chem. 3 (2012) 946–953, https://doi.org/10.1039/c2py00591c.
[33] T.N. Tran, C. Di Mauro, A. Graillot, A. Mija, Chemical Reactivity and the Influence of Initiators on the Epoxidized Vegetable Oil/Dicarboxylic Acid System, Macromolecules 53 (2020) 2526–2538, https://doi.org/10.1021/acs.macromol.9b02700.